

APPLICATION OF ADAPTED-BUBBLES TO THE HELMHOLTZ EQUATION WITH LARGE WAVE NUMBERS IN 2D

Adem Kaya^{a,*}

^a*Institut für Mathematik, Universität Potsdam Karl-Liebknecht-Str. 24-25 14476 Potsdam/Golm Germany*

Abstract

An adapted bubble approach which is a modification of the residual-free bubbles (RFB) method, is proposed for the Helmholtz problem in 2D. A new two-level finite element method is introduced for the approximations of the bubble functions. Unlike the other equations such as the advection-diffusion equation, RFB method when applied to the Helmholtz equation, does not depend on another stabilized method to obtain approximations to the solutions of the sub-problems. Adapted bubbles (AB) are obtained by a simple modification of the sub-problems. This modification increases the accuracy of the numerical solution impressively. The AB method is able to solve the Helmholtz equation efficiently in 2D up to $ch = 3.5$ where c is the wave number and h is the mesh size. We provide analysis to show how the AB method mitigates the pollution error.

Keywords:

Helmholtz equation, adapted bubbles, residual-free bubbles, two-level finite element

1. Introduction

Enriching linear finite element space with *residual-free bubble functions* is a general framework for the discretizations of the problems [10, 3, 12, 19, 14, 13]. These functions strongly satisfy the original differential equations and hence obtaining the bubble functions is generally as difficult as solving the original problem such as the convection-diffusion equation [3]. Unlike it was stated in [11], we will show that this is not the case for the Helmholtz problem. Obtaining the bubble functions on triangular elements is easier than solving the original problem. The standard Galerkin finite element method can be used with a coarse mesh to obtain efficient approximations to the bubble functions.

The residual-free bubbles method produces the exact solution of linear differential equations in the one-dimensional case. However, the method in higher-dimensions is approximate and as we will show for the Helmholtz problem in

*Corresponding author

Email address: kaya@uni-potsdam.de (Adem Kaya)

this article, its contribution to the stabilization of the standard Galerkin method is very poor. We modify the residual-free bubbles (RFB) method in 2D by multiplying the right-hand side of the bubble equations with a constant. This operation impressively increase the accuracy. The new bubbles are no more residual-free and we call them *adapted bubbles* (AB). We provide the optimal values of the constants for the triangular and rectangular elements separately. We apply a two-level finite element method using the standard Galerkin finite element method to get approximations to the bubble functions.

We provide analysis to show how the AB method mitigates the pollution error. To this end, we approximate the bubble functions with piece-wise defined linear functions so-called *pseudo-bubbles*. The analysis give rise to a fourth order finite difference scheme with seven-point stencil for plane waves. It is perfectly applicable in polygonal and triangular domains. We use this method to do comparison with the AB method.

Standard discretizations when applied to the Helmholtz problem suffer from the pollution effect when the wave number is large [2]. Moreover standard iterative solvers are ineffective in obtaining the solutions of the discrete Helmholtz equation [7]. There is a great effort in literature to overcome these difficulties. Among the discretization techniques, there are finite difference [23, 8], finite element [16, 25, 1], discontinuous Galerkin [4, 9], virtual element [20], and boundary element methods [17]. At the same time, there is a great effort to develop efficient preconditioners, such as multigrid [5, 6] and domain decomposition methods [15, 24]. The AB method proposed in this article, does not suffer from the pollution effect for very large wave numbers. It is by far superior than the fourth order accurate scheme proposed here.

The rest of this paper is organized as follows. We review the RFB method for the Helmholtz equation in Section 2. We explain how to implement two-level finite element method in 1D and provide analysis to show the contribution of the bubble functions in reducing the pollution error in Section 3. Section 4 is devoted for the analysis of the RFB method in 2D. We propose the AB method for triangular elements in Section 5. Several numerical experiments are provided in Section 6. The AB method is considered with rectangular elements in Section 7. We finish with concluding remarks in Section 8.

2. Residual-free bubbles method (RFB) for the Helmholtz equation

We start with considering the Helmholtz problem in 1D with Dirichlet boundary conditions on unit interval.

$$\begin{cases} -u'' - c^2 u(x) = f(x), & x \in I \\ u(0) = 0, & u(1) = 1, \end{cases} \quad (1)$$

where we assume that the wave number c is constant. RFB method can be summarized as follows. Let's start with recalling abstract variational formulation of (1): Find $u \in H^1(I)$ such that

$$a(u, v) = (f, v), \quad \forall v \in H^1(I),$$

where

$$a(u, v) = \int_I u'v' dx - c^2 \int_I uv dx$$

and

$$(f, v) = \int_I f v dx.$$

Define $V_h \subset H^1(I)$ as a finite-dimensional space. Then the Galerkin finite element method reads: Find $u_h \in V_h$ such that

$$a(u_h, v_h) = (f, v_h), \quad \forall v_h \in V_h.$$

We now decompose the space V_h as $V_h = V_L \oplus V_B$, where V_L is the space of continuous piecewise linear polynomials and $V_B = \bigoplus_K B_K$ with $B_K = H_0^1(K)$. From this decomposition, every $v_h \in V_h$ can be written in the form $v_h = v_L + v_B$, where $v_L \in V_L$ and $v_B \in V_B$. Bubble component u_B of u_h satisfy the original differential equation in an element K strongly, i.e.

$$\mathcal{L}u_B = -\mathcal{L}u_L + f \quad \text{in} \quad K, \quad (2)$$

subject to boundary condition,

$$u_B = 0 \quad \text{on} \quad \partial K. \quad (3)$$

Since the support of bubble u_B is contained within the element K , we can make a static condensation for the bubble part, getting directly the V_L - projection u_L of the solution u_h [10]. This can be done as follows. Using $V_h = V_L \oplus V_B$, the finite element approximation reads: Find $u_h = u_L + u_B$ in V_h such that

$$a(u_L, v_L) + a(u_B, v_L) = (f, v_L), \quad \forall v_L \in V_L. \quad (4)$$

3. A two level finite element method

In order to find bubble part u_B of the solution, we need to solve (2)-(3). The problems defined by equations (2)-(3) is addressed by solving instead

$$\begin{cases} -\varphi_i'' - c^2\varphi_i = c^2\psi_i & \text{in } K, \quad (i = 1, \dots, n_{en}) \\ \varphi_i = 0 & \text{on } \partial K, \end{cases} \quad (5)$$

and

$$\begin{cases} -\varphi_f'' - c^2\varphi_f = f & \text{in } K, \\ \varphi_f = 0 & \text{on } \partial K. \end{cases} \quad (6)$$

where n_{en} is the number of element nodes. Thus if

$$u_L = \sum_i d_i^K \psi_i, \quad (7)$$

then

$$u_B = \sum_i d_i^K \varphi_i + \varphi_f. \quad (8)$$

Substituting (7) and (8) into (4), we get the matrix formulation

$$\sum_K \sum_i^{n_{en}} d_i^K ((\psi'_i, \psi'_j) - c^2(\psi_i, \psi_j) - c^2(\varphi_i, \psi_j)) = (f, \psi_j) \quad (9)$$

at the global level where d_i are the finite element approximations to the solutions at the nodes.

Numerical solution of the bubble problems (5) and (6) generally requires using a nonstandard method such as for the case of the advection-diffusion equation. This makes the RFB method dependent on another stabilized method when applying it as a two-level finite element method. In [11], the Galerkin-least-squares method (GLS) was used to get approximations to the bubble functions in solving the the Helmholtz equation. Although this is true for the advection-diffusion equation, there is no need to use a nonstandard method to get approximations to the bubble functions when the Helmholtz problem is under consideration. We explain this fact in 1D. It is well known that standard discretizations are effective up to $ch = 0.6$. Suppose that we have a discretization of the domain such that $ch = 0.6$. Even if we use 3 nodes on the sub-domain (element), ch_e (h_e is mesh size on the sub-domain) becomes less than 0.6. If $ch = 3$ on the global mesh, then using 11 nodes for the sub-problems makes $ch_e = 0.3$. More precisely, it

is always true that $ch_e < ch$.

It is true that GLS computation is known to incur at most marginal increase in computational cost over the standard Galerkin method. However, GLS for the sub-problems may lead to misinterpretations related to the bubble functions.

Another way of obtaining the bubble function is to use separation of variables when rectangular elements are used [10]. However, this gives rise to a series solution of the bubble function for which it must be truncated. For a good accuracy, 200 terms are used in [10] which is computationally not so effective. Another drawback is that this approach is limited to the rectangular elements.

3.1. Analysis of the pollution effect of the sub-problems

The inequality $ch_e < ch$ is an indication that the sub-problems are easier to solve; however, we must analyse the pollution effect for the sub-problems for large wave numbers. It is well known that the condition $c^2h < 1$ is sufficient to guarantee that the error of the Galerkin solution is of the same magnitude as the error of the best approximation [2]. This condition is necessary when the size the domain is fixed for increasing c . More precisely, the exact solution is very oscillatory. In our case, the exact solutions of the sub-problems are not oscillatory. When $ch < \pi$, the exact solutions of the sub-problems are always in the form of a half wave as the homogenous Dirichlet boundary condition is applied everywhere on the boundary. When $\pi < ch < 2\pi$, the exact solutions of the sub-problems are always in the form of a single wave. In this regime, the standard Galerkin method is pollution free for the sub-problems for any wave number. Note that, in simulations, 12 nodes per wave is generally chosen which corresponds to $ch \approx 0.62$.

We use the standard Galerkin finite element method with piecewise linear basis functions to approximate the bubble functions. Note that the bubble problems (5) and (6) can be solved independently and hence parallel processors can be used to carry out these computations efficiently. When uniform meshes are used and the right hand side function f is constant, construction of the system matrix is as cheap as construction of the system matrix of the standard Galerkin finite element method.

3.2. Shape of the bubble functions and pseudo-bubbles

We have shown that the RFB method is not dependent on another stabilized method to get approximations to the bubble functions when a two-level finite element method is used due to the non-oscillatory behavior of the exact solutions of the sub-problems. This non-oscillatory behavior of the exact solutions opens a gateway to approximate these bubble functions with piecewise-defined linear simple functions. These approximations are called *pseudo-bubbles* and constructed considering the shape of the bubble functions. Pseudo-bubbles were applied to the advection-diffusion-reaction equation in [22, 21].

Here, we consider the case $ch < \pi$ for which the bubble functions are in the form of a half wave. We present the bubble functions $\varphi_{1,2}$ in Figure 1 for $c = 60, 300$ when $h = 0.01$. Efficient yet cheap approximations to these bubble functions with piecewise-defined linear functions are given in Figure 2. While on the left in Figure 2, two pseudo-bubbles are used, it is possible to approximate $\varphi_{1,2}$ with a single pseudo-bubble. The humps of the bubble functions $\varphi_{1,2}$ come closer as ch increases (see Figure 1). Thus, for larger ch , we can derive more efficient approximations to the bubble functions when a single pseudo-bubble is used. The advantage of using a single pseudo-bubble is that the maximum of the pseudo-bubble occurs in the middle of the element. Applying the minimization technique applied in [22], one can find the optimal heights and locations of the peaks of the pseudo-bubbles. When a single pseudo-bubble is used, one can easily calculate integrals in the finite element formulation. This will be important in modifying the RFB method in 2D.

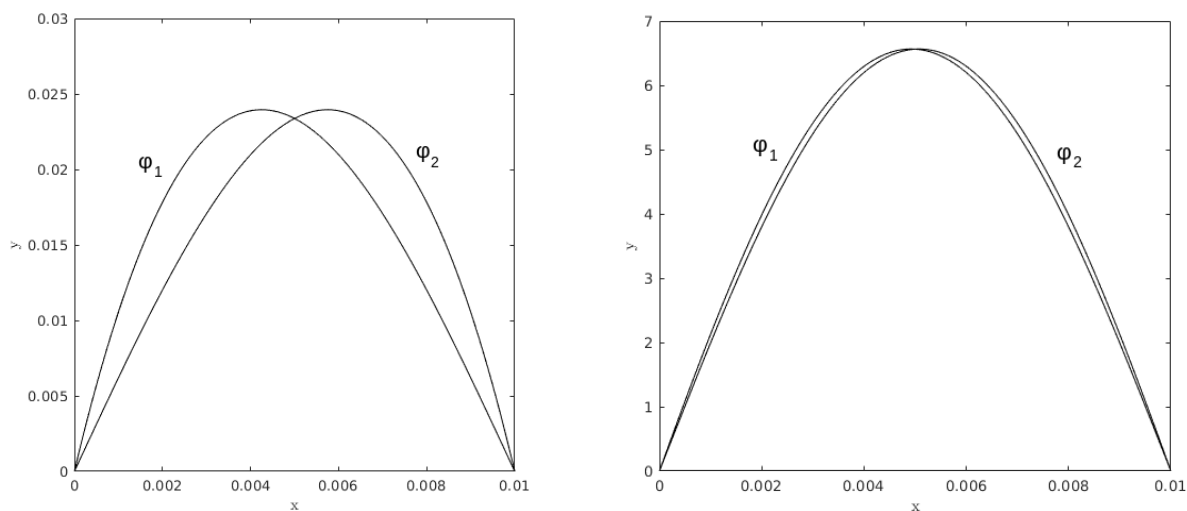


Figure 1: Bubble functions for $c = 60$ (left) and $c = 300$ (right).

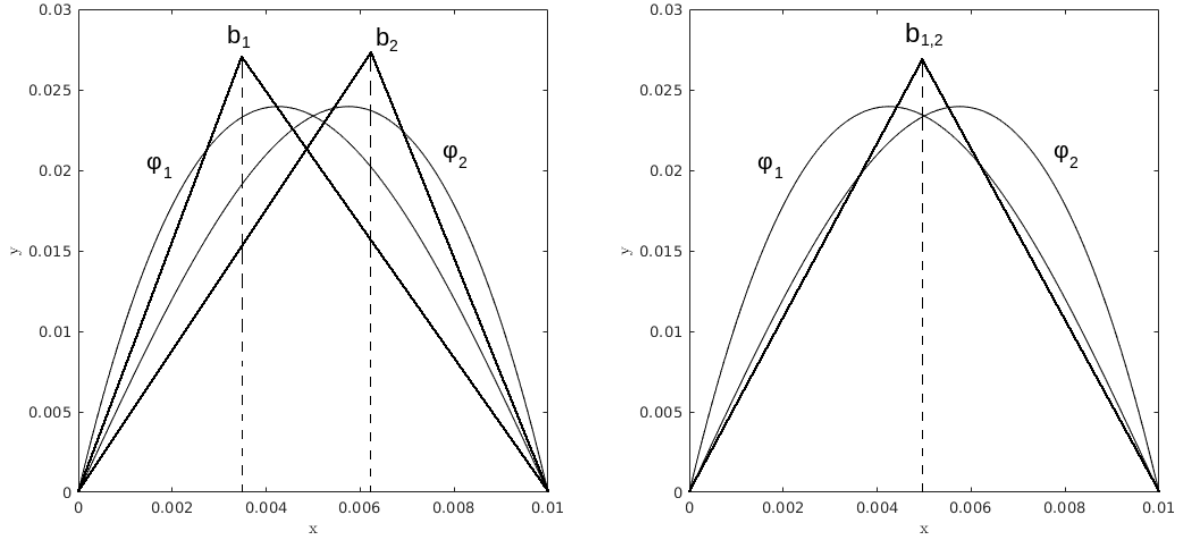


Figure 2: Two different approaches to approximate the bubble functions.

3.3. Analysis of the pseudo-bubbles

In order to see how the residual-free bubbles method overcome the pollution effect, we first consider linear finite element method for (1) when $f(x) = 0$, $u(0) = 0$ and $u(1) = \sin(c)$. The exact solution is $u(x) = \sin(cx)$. We obtain the truncation error and see how the error deteriorates as c increases for fixed ch which is simply the pollution effect. To this end, we jump to the finite difference equivalence of the linear finite method. Let U_j represents the numerical solution and choose n equally distributed nodes for which $h = 1/(n - 1)$. Taking the integrals in linear finite element formulation and scaling by h gives

$$-\frac{U_{j+1} - 2U_j + U_{j-1}}{h^2} - c^2 \frac{U_{j+1} + 4U_j + U_{j-1}}{6} = 0, \quad j = 2, \dots, n - 2. \quad (10)$$

From the boundary conditions,

$$U_1 = 0, \quad U_n = \sin(c).$$

Using the Taylor series expansion, we get the truncation error for (10).

$$\tau(x) = -\frac{c^2 h^2}{6} u'' - \left(\frac{c^2 h^4}{72} + \frac{h^2}{12} \right) u^{(4)} - \frac{h^4}{360} u^{(6)} + O(h^6). \quad (11)$$

The pollution effect can not be seen from (11). To see it, we substitute the exact solution $u(x) = \sin(cx)$ into (11).

$$\tau(x) = \frac{c^4 h^2}{6} \sin(cx) - \left(\frac{c^6 h^4}{72} + \frac{c^4 h^2}{12} \right) \sin(cx) + \frac{c^6 h^4}{360} \sin(cx) + \mathcal{O}(c^8 h^6).$$

Rearranging the above equation gives

$$\tau(x) = \sin(cx) \left(\frac{c^4 h^2}{12} - \frac{c^6 h^4}{90} + \mathcal{O}(c^8 h^6) \right). \quad (12)$$

When the exact solution is oscillatory, that is, c is large, the term $c^4 h^2/12$ in (12) becomes large, that is, $\tau(x)$ is large, even if $ch = \text{constant}$ is small. This is called the pollution effect. When ch is sufficiently small, there is no phase error for the Dirichlet problem when c is large, however when a Neumann or Robin boundary condition is used, phase error is also observed.

The simplest way to mitigate this pollution effect is to choose $c^2 h$ sufficiently small. However, this requires intractable matrices in higher dimensions. The general idea in literature is to decrease the effect of the first few terms in (12) so that tractable matrix sizes can be obtained. For example, using higher order accurate methods of finite difference or higher order polynomials finite element may allow to eliminate the first few terms. If the first term can be eliminated, then the requirement to mitigate the pollution effect reduces to $c^{3/2} h$ being sufficiently small. However, higher order methods generally use more points and this increases the nonzero entries of the matrices.

In order to get a deeper insight of the working principle of the residual-free bubbles method in mitigating the pollution effect, we consider the pseudo-bubbles in Figure 2 on the right. This choice allows us to take the integrals containing the bubble functions, explicitly.

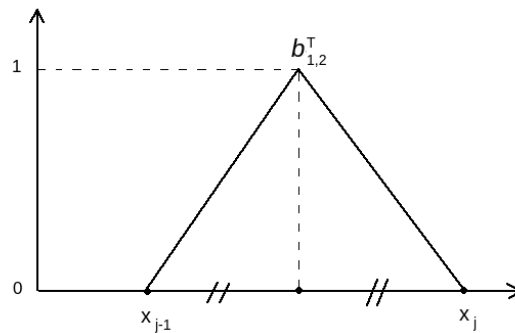


Figure 3: Basis functions employed in the approximation of bubble functions.

We can define the pseudo-bubbles $b_{1,2}$ using the basis functions $b_{1,2}^T$ represented in Figure 3 and heights of $b_{1,2}$,

i.e., $\alpha_{1,2}$. More precisely,

$$b_{1,2} = \alpha_{1,2} b_{1,2}^T, \quad (13)$$

where $\alpha_1 = \alpha_2$. Applying the technique proposed in [22] (set $\xi = h/2, \epsilon = 1, \sigma = -c^2$ in equation (13) in [22]) gives

$$\alpha_1 = \frac{3c^2 h^2}{4(12 - c^2 h^2)}. \quad (14)$$

Taking the integrals in (4) making use of (13) gives the finite difference formula

$$-\frac{U_{j+1} - 2U_j + U_{j-1}}{h^2} - c^2 \frac{U_{j+1} + 4U_j + U_{j-1}}{6} - \alpha_1 c^2 \frac{U_{j+1} + 2U_j + U_{j-1}}{4} = 0, \quad j = 2, \dots, n-2. \quad (15)$$

Using Taylor expansions of $u(x \pm h)$, definition of α_1 given in (14) and the exact solution $u(x) = \sin(cx)$, we obtain the truncation error

$$\tau(x) = \sin(cx) \left(\frac{c^4 h^2}{12} - \frac{c^6 h^4}{90} + O(c^8 h^6) \right) + \sin(cx) \left(-\frac{3c^4 h^2}{4(12 - c^2 h^2)} + \frac{3c^6 h^4}{16(12 - c^2 h^2)} + O(c^8 h^6) \right).$$

Rearranging the right-hand side of the above formula we end up with

$$\tau(x) = \sin(cx) \left(c^4 h^2 \left(\frac{1}{12} - \frac{3}{4(12 - c^2 h^2)} \right) + c^6 h^4 \left(-\frac{1}{90} + \frac{3}{16(12 - c^2 h^2)} \right) + O(c^8 h^6) \right). \quad (16)$$

While the coefficient of $c^4 h^2$ in (12) is $1/12$, the coefficient of $c^6 h^4$ is $1/90$ in magnitude. When $ch < \sqrt{15/2} \approx 2.73$, the coefficient of $c^4 h^2$ in (16) is smaller in magnitude and it is close to zero when $ch \approx \sqrt{3}$. Moreover, when $ch < \sqrt{57/16} \approx 1.88$, the coefficient of $c^6 h^4$ in (16) becomes smaller in magnitude. The approximate bubbles shows how the pollution effect is reduced. It is known that RFB method for 1D linear equations is exact [11]. This means that it automatically makes the coefficient of all powers $c^{n+2} h^n$, $n = 2, 3, \dots$, zero. A good approximation to the residual-free bubbles significantly reduce the pollution effect. The RFB method is approximate in 2D. It is well known that the contributions of the residual-free bubble functions to the stabilization of the Galerkin method is very poor. The observations we made here will be helpful to further increase the accuracy of the method in 2D. We will modify the sub-problems in 2D and use adapted bubbles to further increase the accuracy of the bubble approach.

4. The RFB method in 2D

We have shown that the RFB method is able to solve the Helmholtz problem in 1D cheaply and efficiently for very large wave numbers. As it was stated in [11], RFB method is not as efficient in 2D as in 1D. To show this fact, we

consider the following problem on an equilateral triangular shaped domain with vertices $(0, 0)$, $(0, 1)$ and $(0.5, \sqrt{3}/2)$.

$$\begin{cases} -\Delta u - c^2 u = 0, & \text{in } \Omega, \\ u(x, y) = \sin(cx \sin(\theta) + cy \cos(\theta)), & \text{on } \partial\Omega_D, \end{cases} \quad (17)$$

where the exact solution is $u(x, y) = \sin(cx \sin(\theta) + cy \cos(\theta))$. We use equilateral triangular elements with linear basis functions. We solve the following equations on element level to get the RFB functions.

$$\begin{cases} -\Delta\varphi_i - c^2\varphi_i = c^2\psi_i & \text{in } K, \quad (i = 1, \dots, n_{en}) \\ \varphi_i = 0 & \text{on } \partial K, \end{cases} \quad (18)$$

and

$$\begin{cases} -\Delta\varphi_f - c^2\varphi_f = f & \text{in } K, \\ \varphi_f = 0 & \text{on } \partial K, \end{cases} \quad (19)$$

where $n_{en} = 3$. φ_i and ψ_i , ($i = 1, 2, 3$) are the RFB and the linear basis functions, respectively. Linear finite element method with a coarse mesh can be used to obtain efficient approximations to the bubble functions. To do some analyses, we approximate the RFB functions with piecewise-defined linear functions with the maximum at the centroid of the element. Let $b_{1,2,3} = \alpha_2 b^T$ be the approximation to the bubble functions where b^T is the linear basis bubble function that assumes zero at the vertices of the element and one at the centroid of the element. Applying the same procedure we applied in 1D (see [21] for more details), gives

$$\alpha_2^2 \int_K \nabla b^T \nabla b^T dS - \alpha_2^2 c^2 \int_K b^T b^T dS = \alpha_2 \int_K \psi_i b^T dS, \quad i = 1, 2, 3. \quad (20)$$

Solving the above equation for α_2 and calculating the integrals for ψ_1 gives

$$\alpha_2 = \frac{2c^2 h^2}{3(72 - c^2 h^2)}. \quad (21)$$

Considering 6 adjacent elements as shown in Figure 4, the RFB method is equivalent to the following finite difference scheme.

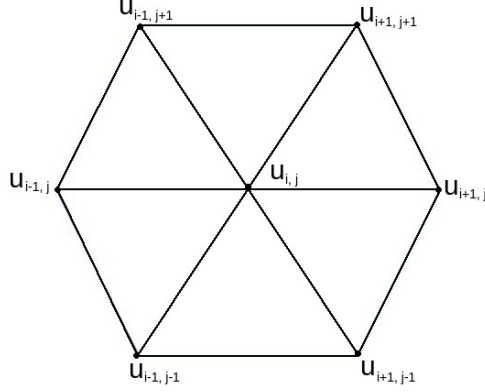


Figure 4: Equilateral triangles surrounding a node.

$$\frac{6U_{i,j}-U_{i-1,j}-U_{i-1,j+1}-U_{i+1,j+1}-U_{i+1,j}-U_{i+1,j-1}-U_{i-1,j-1}}{\sqrt{3}h^2} - c^2 \frac{6U_{i,j}+U_{i-1,j}+U_{i-1,j+1}+U_{i+1,j+1}+U_{i+1,j}+U_{i+1,j-1}+U_{i-1,j-1}}{8\sqrt{3}} - \alpha_2 c^2 \frac{23U_{i,j}+U_{i-1,j}+U_{i-1,j+1}+U_{i+1,j+1}+U_{i+1,j}+U_{i+1,j-1}+U_{i-1,j-1}}{6\sqrt{3}}, \quad i, j = 1, \dots, N_{\text{int}}, \quad (22)$$

where $U_{i,j} \approx u(x, y)$, $U_{i-1,j} \approx u(x-h, y)$, $U_{i-1,j+1} \approx u(x-\frac{h}{2}, y+\frac{\sqrt{3}}{2}h)$, $U_{i+1,j+1} \approx u(x+\frac{h}{2}, y+\frac{\sqrt{3}}{2}h)$, $U_{i+1,j} \approx u(x+h, y)$, $U_{i+1,j-1} \approx u(x+\frac{h}{2}, y-\frac{\sqrt{3}}{2}h)$ and $U_{i-1,j-1} \approx u(x-\frac{h}{2}, y-\frac{\sqrt{3}}{2}h)$. Note that when $\alpha_2 = 0$, (22) is equivalent to the linear finite element method with equilateral triangular element.

To analyse the RFB method, we substitute the Taylor expansions of the exact solution at the grid points. The derivation of the truncation error is given in (23)-(25). In our analysis, we will examine the coefficients of $c^4 h^2$ and $c^6 h^4$ in (25), that is, C_2 and C_1 in (26).

Figure 5 shows the graph of C_1 and C_2 for $\alpha_2 = 0$ (standard Galerkin) and for α_2 in (21) (pseudo-RFB). We set $\theta = \pi/3$ to plot the graph of C_2 . The slight decreases in C_1 and C_2 in magnitude for $0 < ch < 3$, explains why the RFB method is not effective in 2D.

$$\begin{aligned}
\tau(x, y) = & \frac{6u(x, y) - u(x-h, y) - u(x+\frac{\sqrt{3}}{2}h) - u(x+\frac{h}{2}, y + \frac{\sqrt{3}}{2}h) - u(x+h, y) - u(x+\frac{h}{2}, y - \frac{\sqrt{3}}{2}h) - u(x+h, y) + u(x+\frac{h}{2}, y - \frac{\sqrt{3}}{2}h) + u(x-\frac{h}{2}, y - \frac{\sqrt{3}}{2}h)}{8\sqrt{3}} \\
& - c^2 \alpha_2 \frac{3u(x, y) + u(x-h, y) + u(x+\frac{\sqrt{3}}{2}h) + u(x+\frac{h}{2}, y + \frac{\sqrt{3}}{2}h) + u(x+h, y) + u(x+\frac{h}{2}, y - \frac{\sqrt{3}}{2}h) + u(x-h, y) + u(x-\frac{h}{2}, y - \frac{\sqrt{3}}{2}h)}{\sqrt{3}h^2} = \\
& - \frac{189h^4 u^{(0,6)}(x, y) + 945h^4 u^{(2,4)}(x, y) + 15120h^2 u^{(4,2)}(x, y) + 7560h^2 u^{(6,0)}(x, y) + 15120h^2 u^{(2,2)}(x, y) + 120960u^{(0,2)}(x, y) + 120960u^{(2,0)}(x, y)}{6\sqrt{3}} \\
& - \frac{c^2 (h^2 (7560h^2 u^{(0,4)}(x, y) + 15120h^2 u^{(2,2)}(x, y) + 7560h^2 u^{(4,0)}(x, y) + 120960u^{(0,2)}(x, y) + 120960u^{(2,0)}(x, y)) + 967680u(x, y)}{80640\sqrt{3}} \\
& - \frac{\alpha_2 c^2 (h^2 (7560h^2 u^{(0,4)}(x, y) + 15120h^2 u^{(2,2)}(x, y) + 7560h^2 u^{(4,0)}(x, y) + 120960u^{(0,2)}(x, y) + 120960u^{(2,0)}(x, y)) + 725760u(x, y)}{483840\sqrt{3}} + O(h^5).
\end{aligned} \tag{23}$$

Since

$$\frac{120960u^{(0,2)}(x, y) + 120960u^{(2,0)}(x, y)}{80640\sqrt{3}} - \frac{967680u(x, y)}{645120\sqrt{3}} = 0,$$

(23) becomes

$$\begin{aligned}
\tau(x, y) = & - \frac{189h^4 u^{(0,6)}(x, y) + 945h^4 u^{(2,4)}(x, y) + 315h^4 u^{(4,2)}(x, y) + 231h^4 u^{(6,0)}(x, y) + 7560h^2 u^{(0,4)}(x, y) + 15120h^2 u^{(2,2)}(x, y) + 7560h^2 u^{(4,0)}(x, y)}{c^2 (7560h^2 u^{(0,4)}(x, y) + 15120h^2 u^{(2,2)}(x, y) + 7560h^2 u^{(4,0)}(x, y) + 120960u^{(0,2)}(x, y) + 120960u^{(2,0)}(x, y))} \\
& - \frac{645120\sqrt{3}}{80640\sqrt{3}} \\
& - \frac{\alpha_2 c^2 (h^2 (7560h^2 u^{(0,4)}(x, y) + 15120h^2 u^{(2,2)}(x, y) + 7560h^2 u^{(4,0)}(x, y) + 120960u^{(0,2)}(x, y) + 120960u^{(2,0)}(x, y)) + 725760u(x, y)}{483840\sqrt{3}} + O(h^5).
\end{aligned} \tag{24}$$

Substituting the exact solution $u(x, y) = \sin(c \cos(\theta)x + c \sin(\theta)y)$ (note that more general solutions can be chosen) into (24) gives

$$\begin{aligned}
\tau(x, y) = & - \frac{1}{322560\sqrt{3}} (c^2 (35c^5 h^5 \cos(cx \cos(\theta) + cy \sin(\theta) + \theta) + 21c^5 h^5 \cos(cx \cos(\theta) + cy \sin(\theta) + 3\theta) + 7c^5 h^5 \cos(cx \cos(\theta) + cy \sin(\theta) + 5\theta) + \\
& c^5 h^5 \cos(cx \cos(\theta) + cy \sin(\theta) + 7\theta) + 35c^5 h^5 \cos(-cx \cos(\theta) - cy \sin(\theta) + \theta) + 21c^5 h^5 \cos(-cx \cos(\theta) - cy \sin(\theta) + 3\theta) + 7c^5 h^5 \cos(-cx \cos(\theta) - cy \sin(\theta) + 5\theta) + \\
& c^5 h^5 \cos(-cx \cos(\theta) - cy \sin(\theta) + 7\theta) + 5040\alpha_2 c^4 h^4 \sin(cx \cos(\theta) + cy \sin(\theta)) + 2940c^4 h^4 \sin(cx \cos(\theta) + cy \sin(\theta)) - 42c^4 h^4 \sin(cx \cos(\theta) + cy \sin(\theta) + 6\theta) + \\
& 42c^4 h^4 \sin(-cx \cos(\theta) - cy \sin(\theta) + 6\theta) - 80640\alpha_2 c^2 h^2 \sin(cx \cos(\theta) + cy \sin(\theta)) - 30240c^2 h^2 \sin(cx \cos(\theta) + cy \sin(\theta)) + 483840\alpha_2 \sin(cx \cos(\theta) + cy \sin(\theta)) + O(h^5).
\end{aligned} \tag{25}$$

The last 6 terms in (25) can be written in the form

$$\sin(cx \cos(\theta) + cy \sin(\theta)) \left(c^6 h^4 \underbrace{\frac{-2940 + \frac{80640\alpha_2}{c^2} + 84 \cos(6\theta)}{322560\sqrt{3}}}_{C_2} + c^4 h^2 \underbrace{\frac{30240 - \frac{483840\alpha_2}{c^2 h^2}}{322560\sqrt{3}}}_{C_1} \right). \tag{26}$$

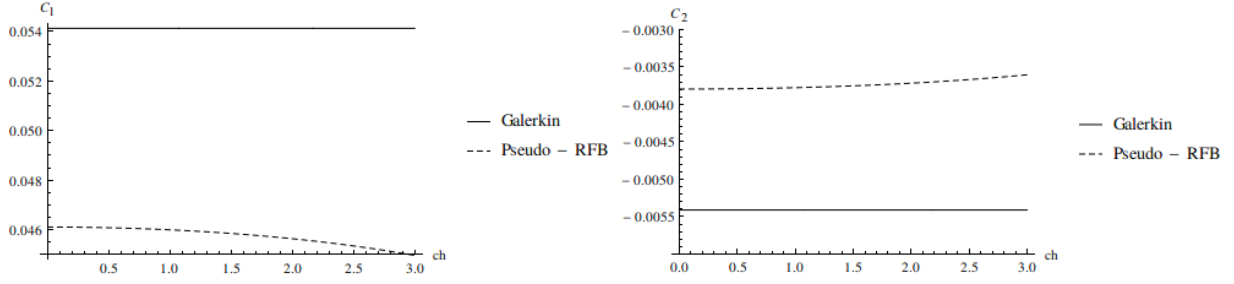


Figure 5: Comparison of the linear Galerkin method and the pseudo-RFB method for the coefficients C_1 (left) and C_2 (right).

One way to improve the accuracy of the bubble approach in 2D is to modify the right-hand side of the bubble equations in (18) by multiplying with a constant, say μ . Then, α_2 becomes

$$\alpha_2 = \frac{2\mu c^2 h^2}{3(72 - c^2 h^2)}.$$

After this modification, the bubble functions are no more residual-free. We call these modified functions as *adaptive bubble* functions. We call the piecewise-defined linear approximations to these adaptive bubble functions as *pseudo-adaptive bubble* functions.

We give two examples here to validate the approach. Figure 6 shows the graph of C_1 and C_2 when $\mu = 6.8$. It is clear that C_1 is decreased in magnitude substantially. It is almost zero when ch is close to zero. There is not much change in C_2 in magnitude.

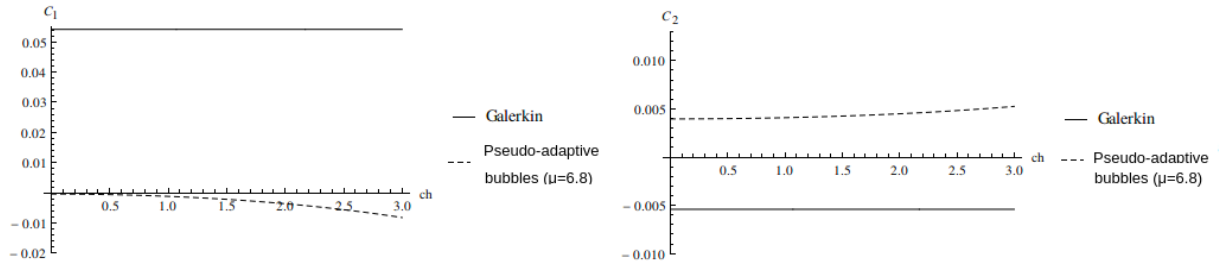


Figure 6: Comparison of the linear Galerkin method and the pseudo-adaptive bubbles method ($\mu = 6.8$) for the coefficients C_1 (left) and C_2 (right).

For the second example, consider $\alpha_2 = 0.0625c^2h^2$ which makes C_1 zero for all values of ch . In this case, the finite difference scheme in (22) is a fourth order scheme with seven points for plane waves. Figure 7 shows the graph of C_1 and C_2 when $\alpha_2 = 0.0625c^2h^2$. While C_1 is zero for all values of ch , there is only a slight change in C_2 in magnitude. This fourth order accurate finite difference scheme can be easily applied in triangular, trapezoidal and polygonal domains. Our main aim in this article is to propose adaptive bubbles approximated by standard Galerkin method. However, the above two method will be used to compare the success of the AB method.

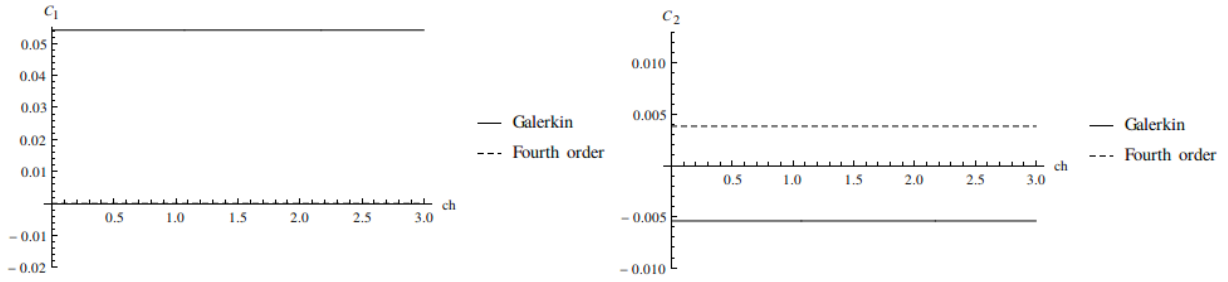


Figure 7: Comparison of the linear Galerkin method and the fourth order accurate method for the coefficients C_1 (left) and C_2 (right).

5. Adaptive bubbles (AB) in 2D with triangular elements

We have shown using the pseudo-bubbles and the truncation error that the RFB method is not effective in 2D. However, it is possible to increase its accuracy with a simple modification, that is, multiplying the right-hand side of the bubble problems with a constant. We proposed two methods using this approach; a pseudo-adaptive bubbles method and a fourth order accurate finite difference scheme that uses seven points. However, our main aim is to obtain more accurate solutions by approximating the adaptive bubble functions with linear finite element method on a coarse mesh.

We follow an empirical way to determine the optimal values of μ_i for varying cm_i where m_i is the median of the global triangular element (see Figure 8, (left)). This is actually a necessity because we have to use a coarse mesh for the sub-problems and shapes of the bubble functions may change significantly when a small change occurs in the number of mesh used for the sub-problems.

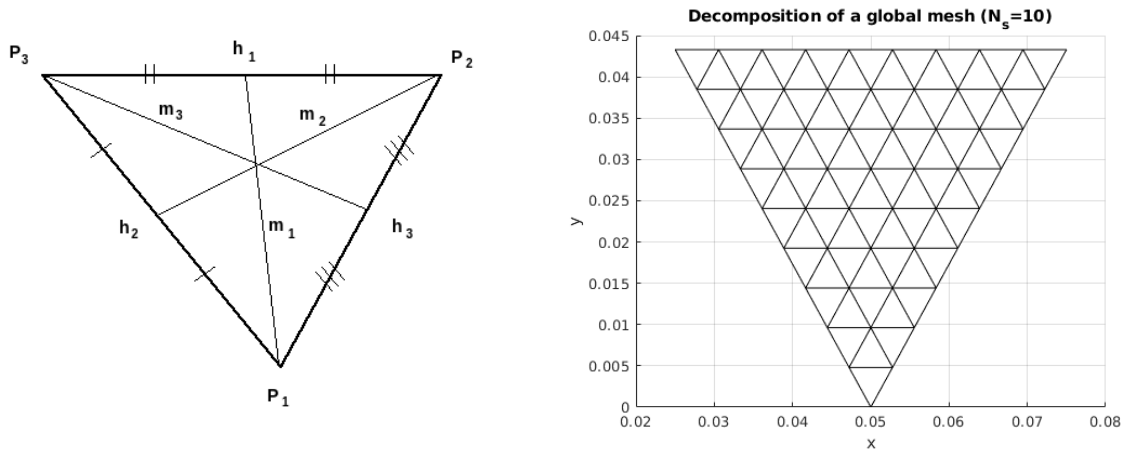


Figure 8: A global mesh (left) and a decomposition of a global mesh with triangular elements when $N_s = 10$ (right).

Considering the problem in (17), we report the optimal values of μ_i ($i = 1, 2, 3$) for different values of cm_i in Table

1 for an equilateral triangular element. The optimality criterion in determining these values is minimization of the error in infinity norm by doing many tests. The values of μ_i are optimal for $\theta = 0, \pi/3, 3\pi/2$. We decompose each global mesh into triangular elements by choosing N_s uniformly distributed nodes on all edges of a triangular element (see Figure 8). We set $N_s = 10$ when $cm_i \leq 2.577$ and set $N_s = 15$ when $cm_i > 2.577$. While choosing $N_s = 10$ amounts to 28×28 matrices, choosing $N_s = 15$ amounts to 78×78 matrices on element level. It is possible to choose smaller values of N_s , especially for smaller ch , but one has to report more optimal values of μ in this case.

Table 1: Optimal values of μ_i for varying cm_i ($i = 1, 2, 3$) when $\theta = 0, \pi/3, 3\pi/2$.

cm_i	μ_i	N_s	cm_i	μ_i	N_s
≤ 0.57	5.4	10	1.933	6.75	10
0.583	5.43	10	2.004	6.9	10
0.644	5.45	10	2.076	7.05	10
0.71	5.5	10	2.147	7.2	10
0.7876	5.5	10	2.219	7.35	10
0.859	5.51	10	2.291	7.52	10
0.893	5.58	10	2.362	7.7	10
0.930	5.6	10	2.434	7.9	10
1.002	5.65	10	2.505	8.05	10
1.074	5.7	10	2.577	8.3	10
1.145	5.75	10	2.577	7.8	15
1.217	5.8	10	2.649	7.95	15
1.288	5.87	10	2.72	8.1	15
1.360	5.95	10	2.75	8.21	15
1.431	6.05	10	2.79	8.25	15
1.503	6.1	10	2.863	8.4	15
1.575	6.17	10	2.93	8.5	15
1.646	6.3	10	3.007	8.55	15
1.718	6.4	10	3.078	8.6	15
1.789	6.5	10	3.15	8.65	15
1.861	6.6	10			

When cm_i is between any of the successive two values in Table 1, we use linear interpolation to get μ_i . When shape of the global mesh changes, the bubble functions behave differently, and hence it becomes more difficult to find the optimal values of μ_i for each bubble functions. We therefore expect deterioration of the AB method when nonuniform mesh is used, especially for large wave numbers. Rectangular elements require solving 5 different bubble problems on each element and hence it becomes more complicated to determine the optimal values of μ_i on nonuniform mesh. Hence, we expect the triangular elements to be more efficient than the rectangular elements on nonuniform mesh.

Remark 1. The optimal values in Table 1 were determined when $\theta = 0$ and hence they are true values for $\theta = \pi/3, 2\pi/3$. The optimal values can be find for other values of θ . We will show by numerical test that the values of μ_i

in Table 1 can be used in any direction when $ch < 1$. It is possible to obtain good approximations up to $ch = 2$ in any direction when $c < 200$.

Remark 2. When $cm_i < 0.57$ (i.e. $ch < 0.65$) the optimal values in any direction are same, that is, $\mu = 5.4$. In simulations, 10 nodes per wave are generally used which corresponds to $ch \approx 0.625$. In this regime, there is only one parameter that we must use, that is, $\mu = 5.4$. Since it works for every direction, we expect the AB method works efficiently when the solution is not a plane wave or an unstructured mesh is used.

To verify the optimal values in Table 1, we use the pseudo-adaptive bubbles. For example, for $\mu = 5.4$ (when $ch < 0.65$), $\alpha_2 = 10.8c^2h^2/(3(72 - c^2h^2))$. Graphs of the coefficients C_1 and C_2 are provided in Figure 9. It is obvious that both C_1 and C_2 are decreased in magnitude which is a verification that the AB method can mitigate the pollution effect substantially.

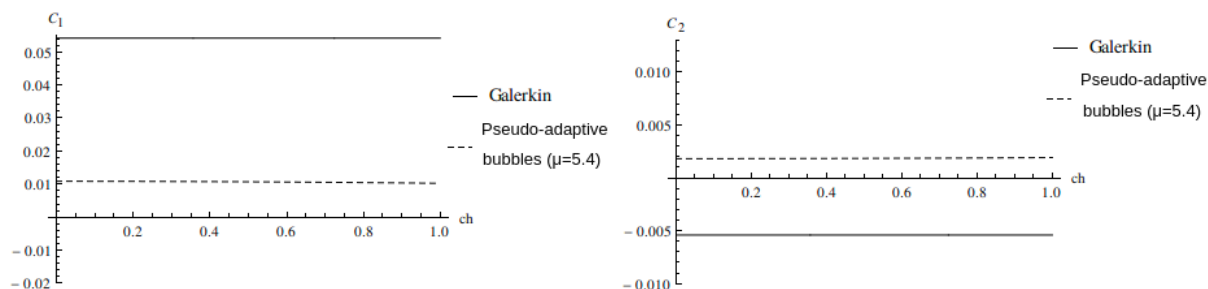


Figure 9: Comparison of the linear Galerkin method and the pseudo-adaptive bubbles method ($\mu = 5.4$) for the coefficients C_1 (left) and C_2 (right).

6. Numerical experiments

In this section, we provide numerical tests to assess the success of the AB method. We compare the AB method with the pseudo-adaptive bubbles ($\mu = 6.8$) (PAB), RFB, fourth order and standard linear Galerkin methods. We use standard linear Galerkin method to approximate the bubble functions for the AB and RFB methods.

6.1. Numerical test 1

We consider the Helmholtz problem in (17). Equilateral triangular elements are used to decompose the domain. We consider the cases $ch = 0.625, 1, 1.75$ when $\theta = 0, \pi/4$ for increasing wave number to compare the methods in mitigating the pollution effect. Figure 10, 11 and 12 show the log-log plots of the error in infinity norm for $ch = 0.625$, $ch = 1$ and $ch = 1.75$, respectively. It is obvious that the AB method is better by far. The RFB method has very small contribution in stabilization of the standard Galerkin method. The PAB method outperforms the fourth order scheme. Moreover, the pollution error for the pseudo-bubbles method and the fourth order scheme is not negligible, particularly when $ch = 1, 1.75$.

Furthermore, we report errors for the M-RFB method in infinity norm for $c = 50$ and varying θ and ch in Figure 13. It is clear that the direction of the plane waves has no importance in the error for $ch \leq 1$. One of the important observation is that the errors are almost same for $\theta = 0, \pi/3, 2\pi/3$. A reasonable explanation for this is that $\cos(6x)$ appears as coefficient of $c^6 h^4$ in the truncation error in C_2 in (26). This is directly related to the topology of the mesh. We can not expect the same behavior for rectangular elements.

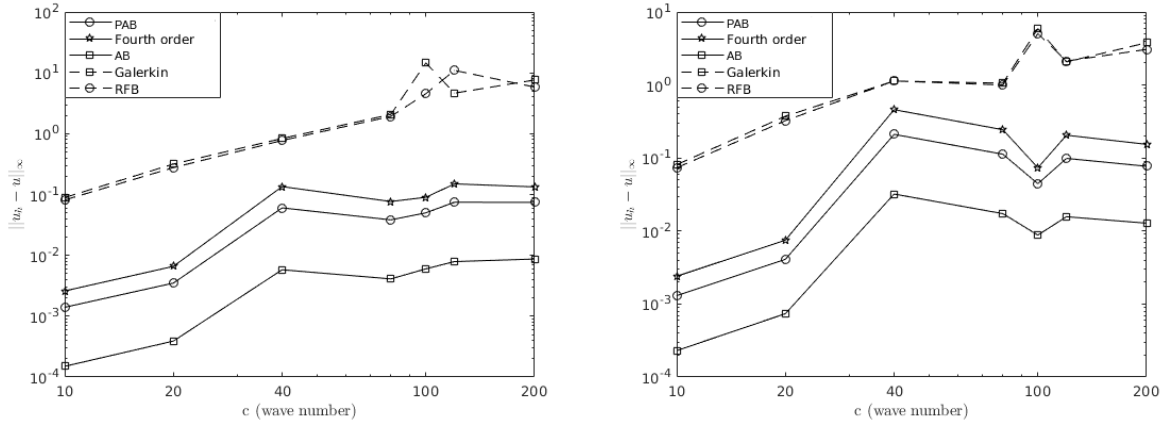


Figure 10: Comparison of the methods when $ch = 0.625$ for $\theta = \pi/4$ (left) and $\theta = 0$ (right).

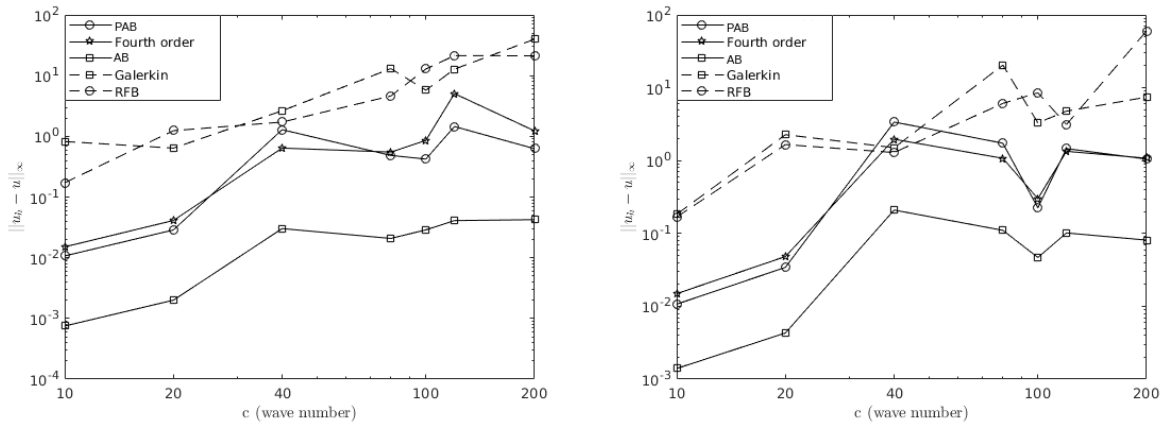


Figure 11: Comparison of the methods when $ch = 1$ for $\theta = \pi/4$ (left) and $\theta = 0$ (right).

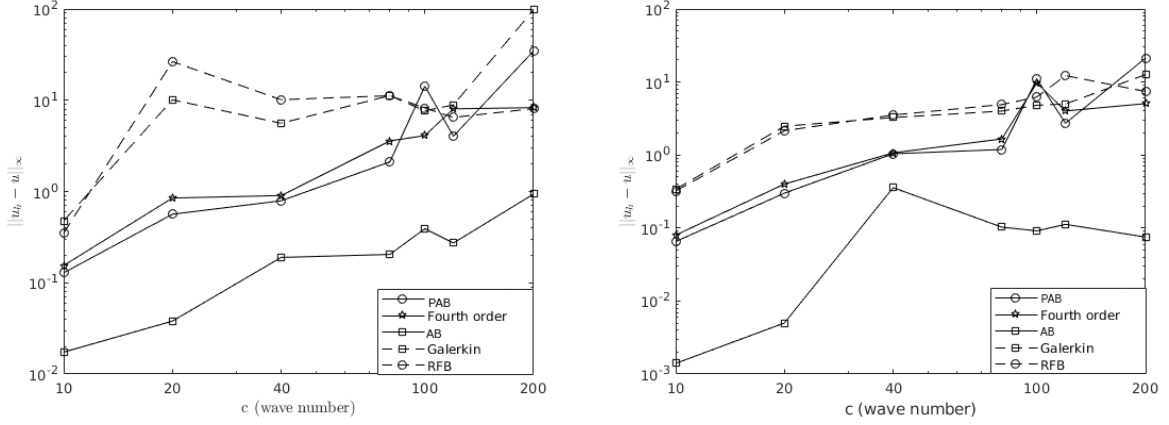


Figure 12: Comparison of the methods when $ch = 1.75$ for $\theta = \pi/4$ (left) and $\theta = 0$ (right).

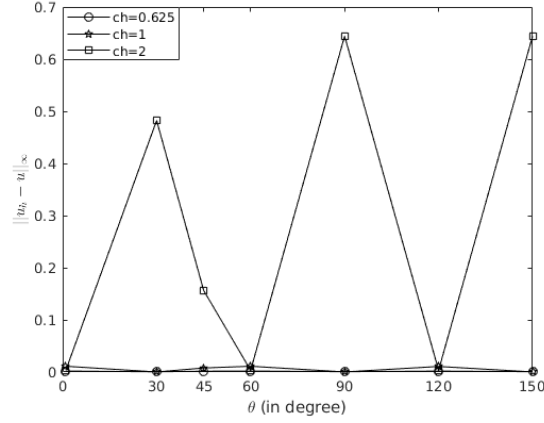


Figure 13: Error versus θ for the AB method when $c = 50$.

6.2. Numerical test 2: Neumann boundary condition

We consider the following Helmholtz problem where homogenous Neumann boundary condition is imposed on a part of the boundary.

$$\begin{cases} -\Delta u - c^2 u = 0, & \text{in } \Omega, \\ u(x, y) = \sin(cx), & \text{on } \partial\Omega_D, \\ \frac{\partial u}{\partial \mathbf{n}} = 0, & \text{on } \partial\Omega_N, \end{cases} \quad (27)$$

where Ω , $\partial\Omega_D$ and $\partial\Omega_N$ are depicted in Figure 14. Exact solution of (27) is $u(x, y) = \sin(cx)$. To see the matrix formulation of the RFB method with Neumann boundary condition, we refer to [10]. We decompose the domain with 400 equilateral triangular elements (see Figure 14).

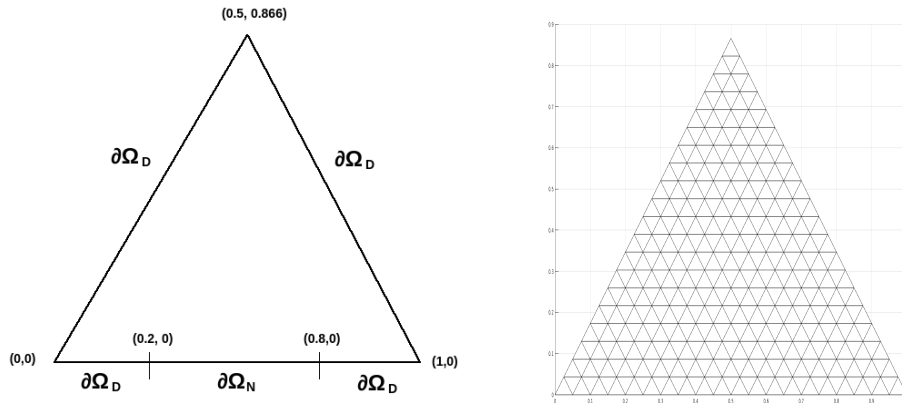


Figure 14: Configuration of the domain in 2D (left) and its triangulation with equilateral triangular shaped elements (right).

We now test the AB method with different values of ch . First, we report numerical results on a fixed uniform mesh (see Figure 14 (right)) for varying wave number c . Figures 15 represents contour plots of the approximate solutions and of the exact solutions for $ch = 0.7, 2.55, 3.5$. We also report maximum and minimum values of the solutions on the graphs. Second, we report numerical results for fixed wave number c on different meshes. Figure 16 shows contour plots of the solutions and meshes used.

The results show that the AB method is very effective on uniform mesh up to $ch = 3.50$. Finally, we report errors in infinity norm in Figure 17 for the AB method up to $ch = 3.5$ on a different mesh where 196 equilateral triangular elements are used. We calculated the error at many points. All the results above verify the robustness of the method in terms of the parameters proposed in Table 1.

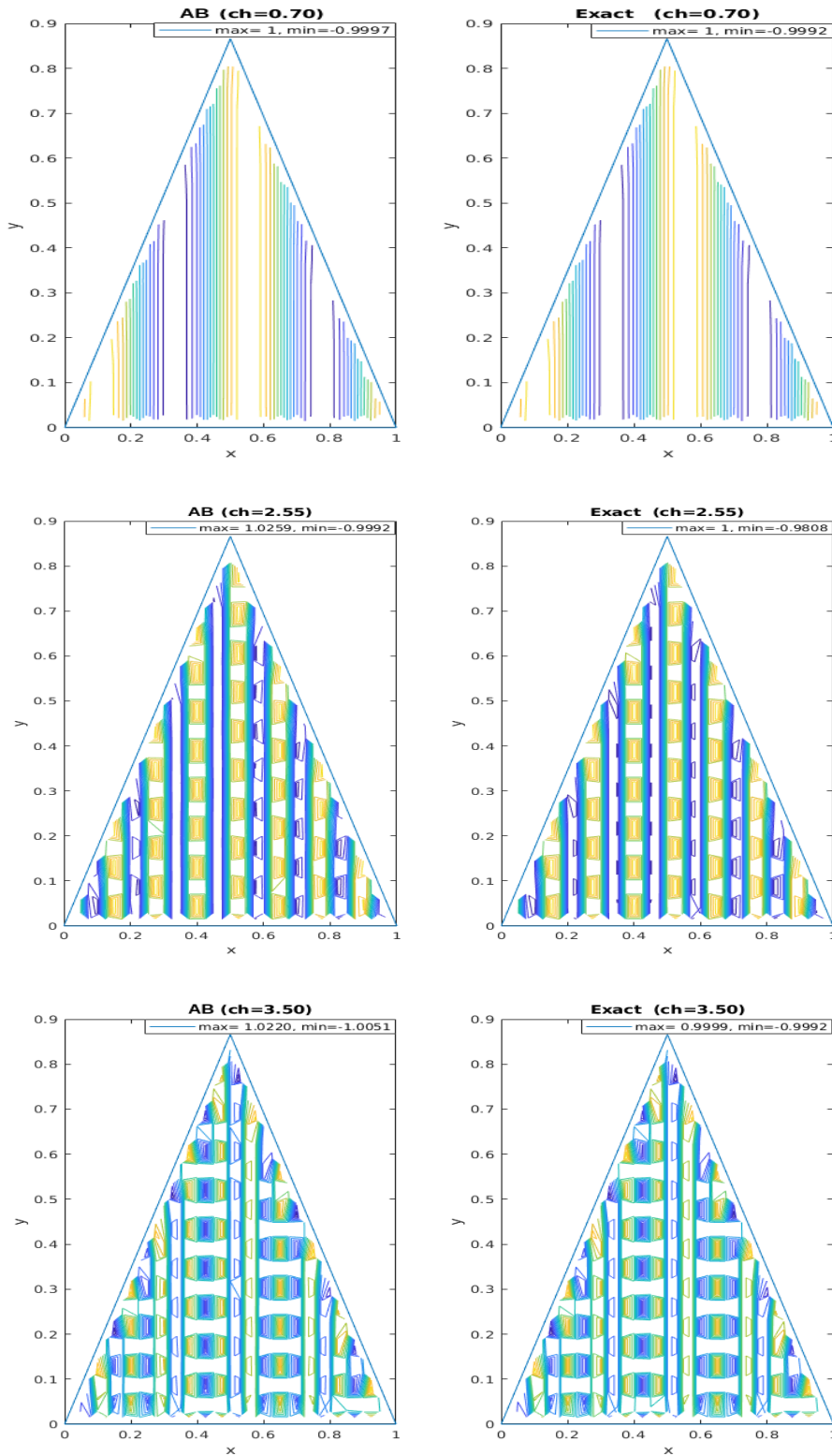


Figure 15: Contour plots of the approximate solutions obtained by the AB method and of the exact solutions for $ch = 0.70, 2.55, 3.50$.

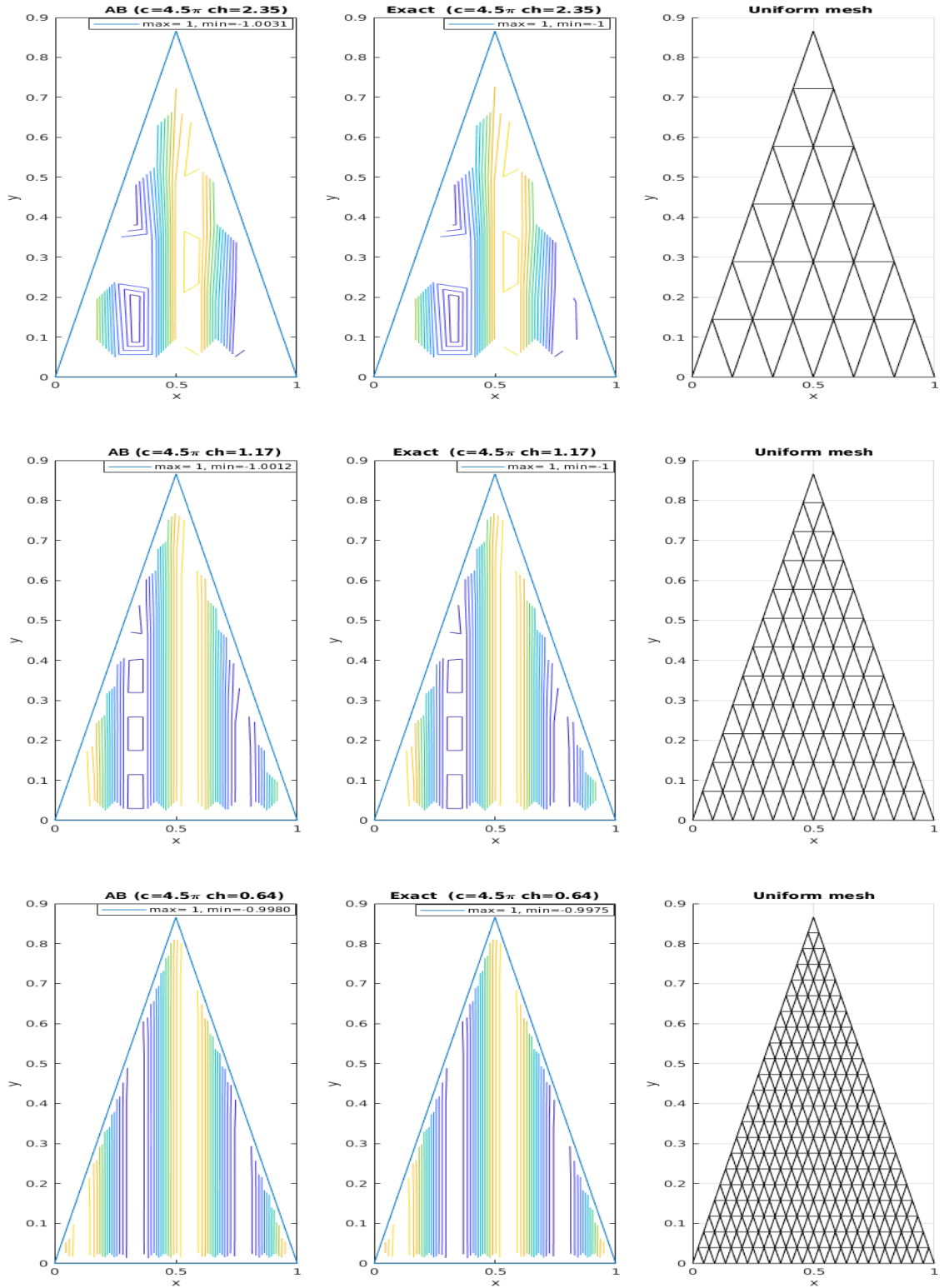


Figure 16: Contour plots of the approximate solutions obtained by the AB method on different meshes and of the exact solutions on the same mesh when $c = 4.5\pi$.

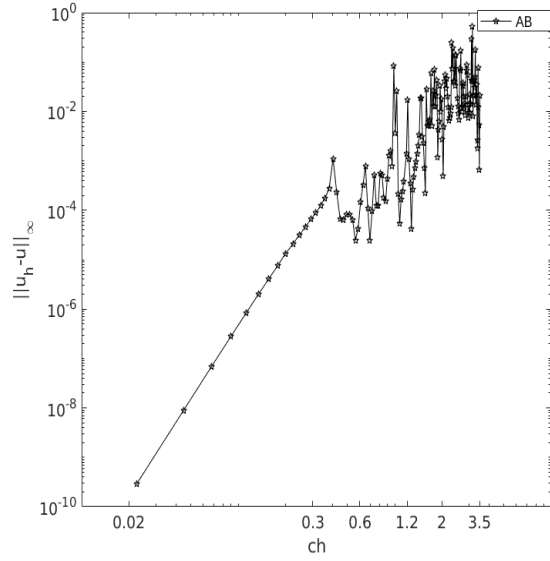


Figure 17: Errors in infinity norm for the AB method up to $ch = 3.5$.

6.3. Numerical test 3: Robin boundary condition and external source

We test the AB method when Robin boundary condition is imposed on a part of the boundary of the domain. We consider

$$\begin{cases} -\Delta u - c^2 u = \sin(x), & \text{in } \Omega, \\ u(x, y) = 0.1, & \text{on } \partial\Omega_D, \\ \frac{\partial u}{\partial \mathbf{n}} = iu, & \text{on } \partial\Omega_R, \end{cases} \quad (28)$$

where $c = 20$, and Ω , Ω_D and Ω_R are represented in Figure 18 (left). As a reference solution, we get a solution using standard Galerkin method on a fine mesh where 40000 uniform triangular elements are used for which $ch = 0.1$. Figure 18 (right) shows the contour plot of the real part of the solution. We show contour plots of the real part of the solutions obtained by the AB method for $ch = 0.5, 1, 2$ in Figure 19. Moreover, we show the corresponding meshes and report the maximum and minimum values of the approximate solutions. Results show that the AB method shows the characteristics of the reference solution for all cases. This is important in application of the multigrid method as a solver.

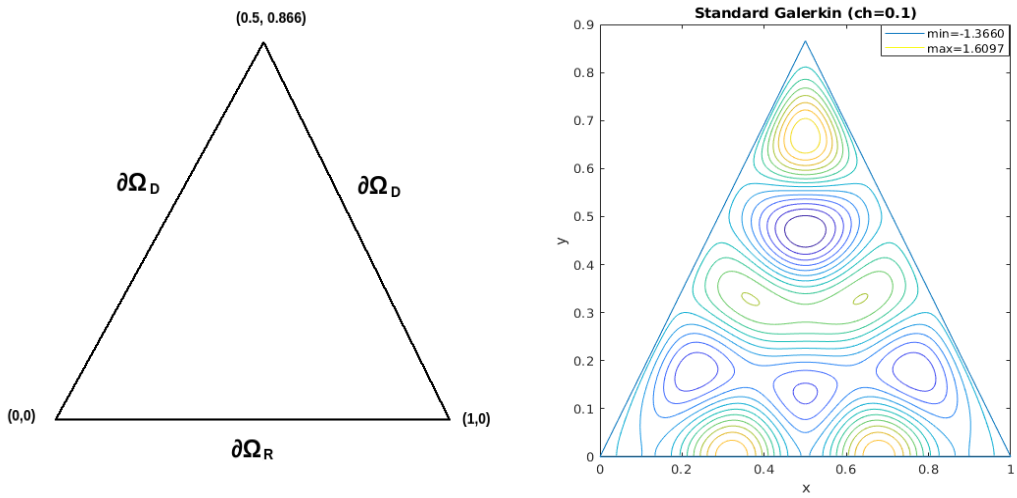


Figure 18: Problem configuration (left) and a reference solution (right) obtained with standard Galerkin method with 40000 uniform triangular elements for which $ch = 0.1$.

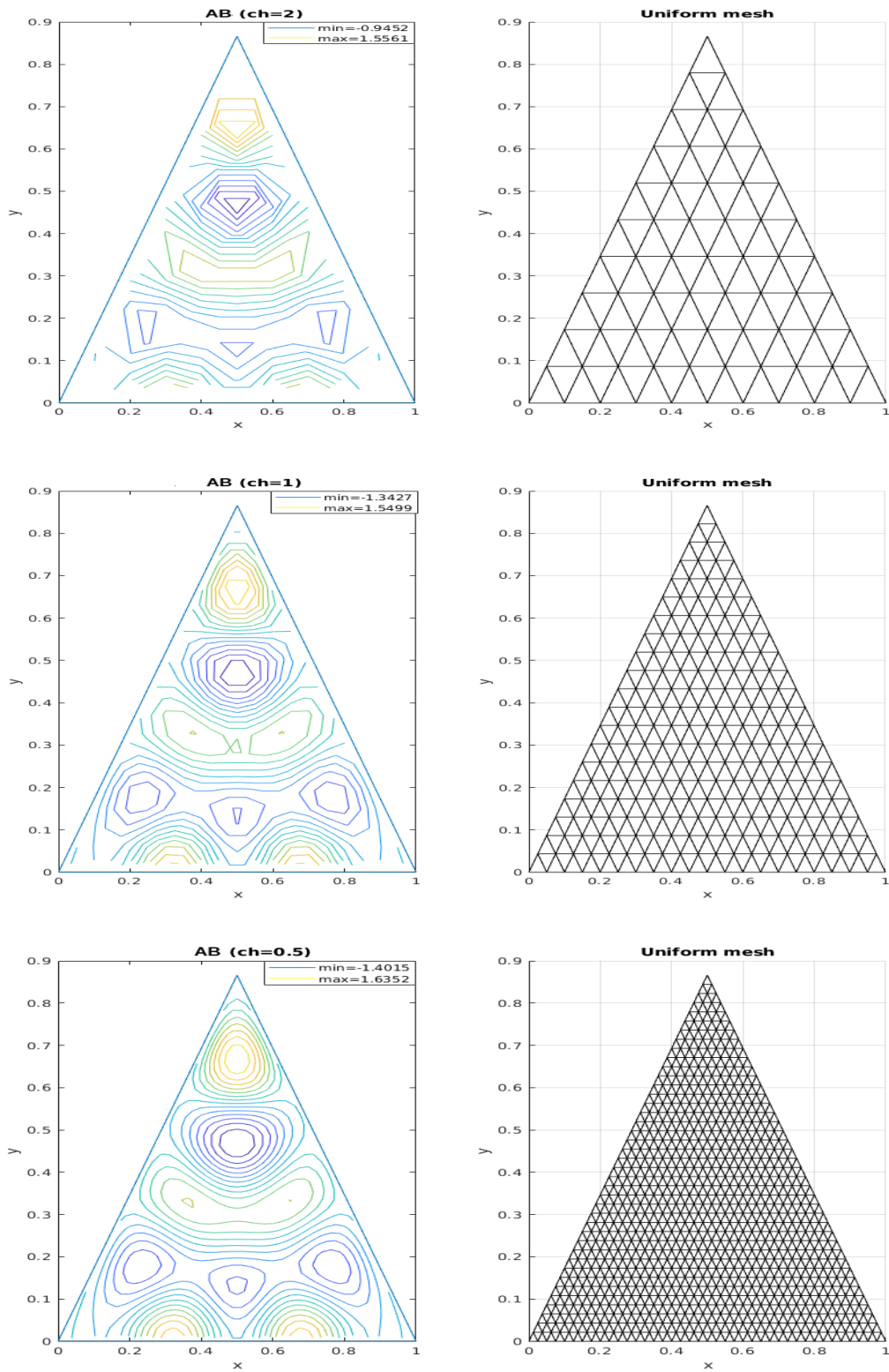


Figure 19: Contour plots of the approximate solutions obtained by the M-RFB method when $c = 20$ using different meshes ($ch = 0.5, 1, 2$).

6.4. Numerical test 4: L-shaped domain and a different triangulation

In this test problem, we change the domain and use a different triangulation. We use a L-shaped domain with the vertices $(-1, -1)$, $(-1, 1)$, $(1, 1)$, $(0, 1)$, $(0, 0)$ and $(-1, 0)$. To decompose the domain, the following Matlab code is used for which $ch \approx 0.625$.

$$\left\{ \begin{array}{l} model = createpde(1); \\ geometryFromEdges(model, @lshapeg); \\ generateMesh(model, 'GeometricOrder', 'linear', 'Hmax', 0.625/c, 'Hmin', 0.625/c); \end{array} \right. \quad (29)$$

The mesh for the case $c = 3.5\pi$ can be seen in Figure 20. We consider the Dirichlet problem in (17) for $\theta = \pi/3$. Figure 20, 21 show the plots of the exact and approximate solutions obtained by the AB, PAB and RFB methods for $c = 3.5\pi$ and $c = 16.5\pi$, respectively. We also report the maximum and minimum values of the approximate solutions on the graphs. Results show that the AB method is better by far especially for larger wave number. Furthermore, we give the plots of the exact solution and approximate solution for AB given in Figure 22. We did not report solutions for the PAB and RFB methods as their results are no more related to the exact solution.

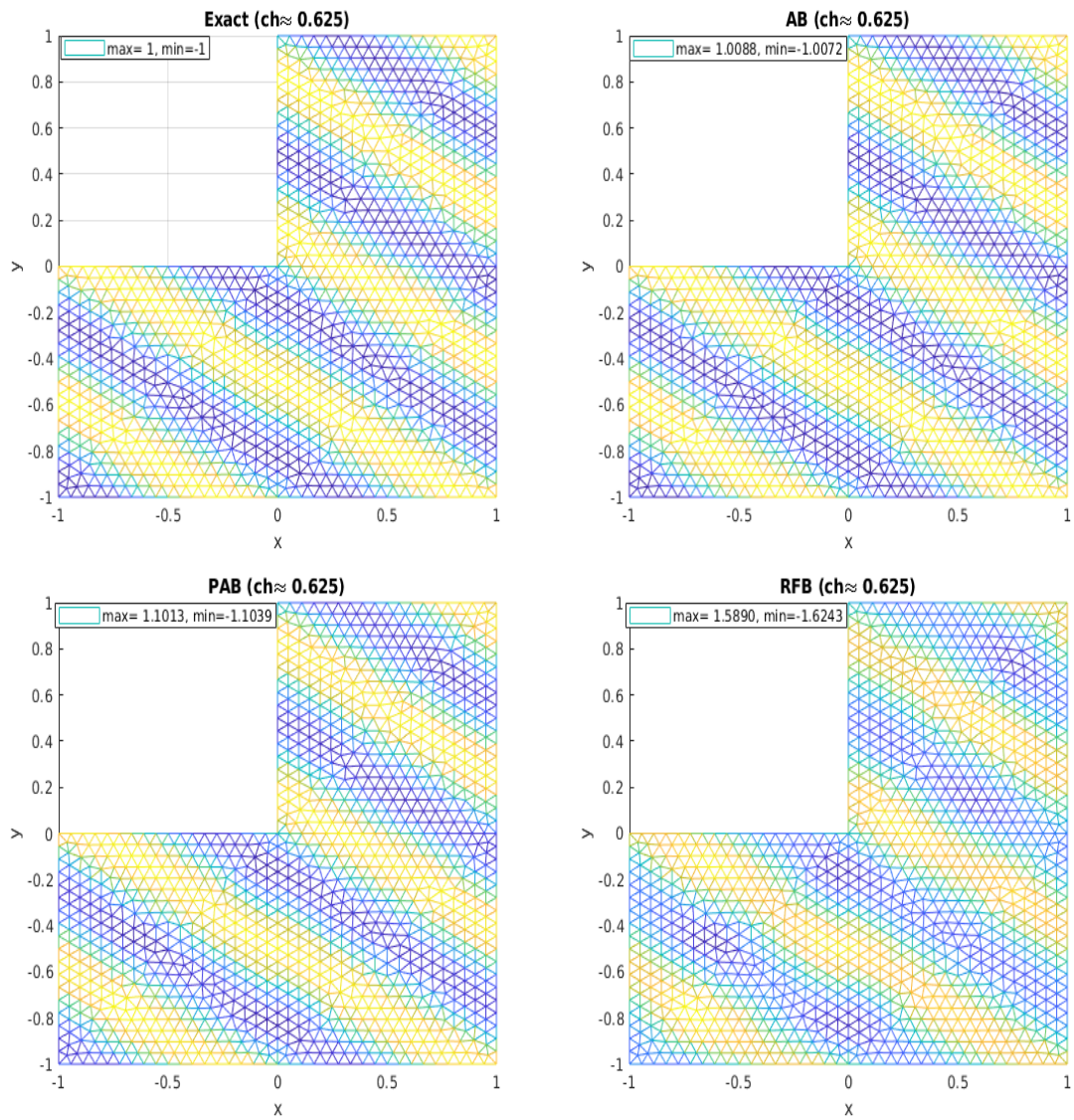


Figure 20: Plots of the exact and approximate solutions obtained by the AB, PAB and RFB methods when $c = 3.5\pi$.

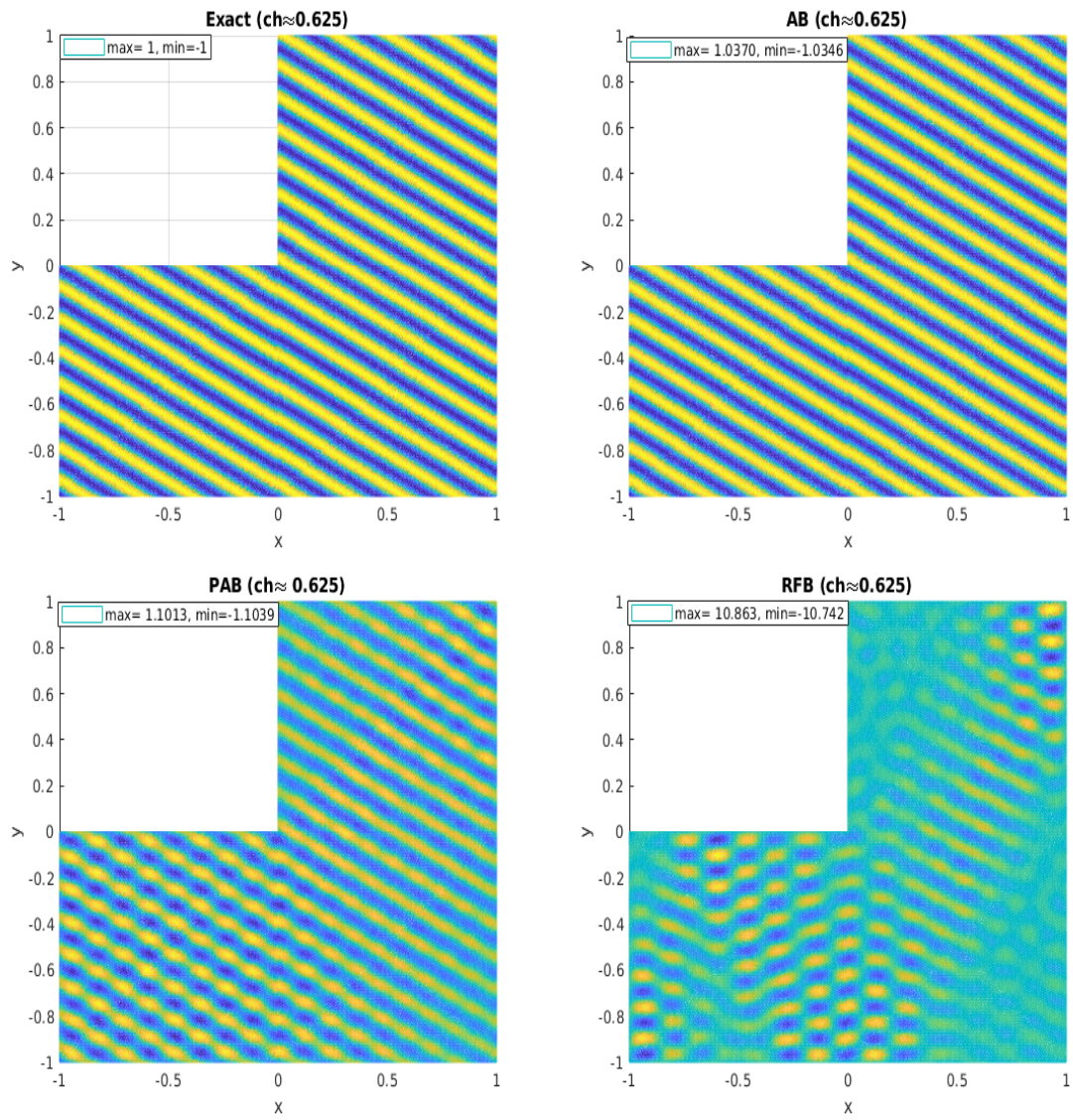


Figure 21: Plots of the exact and approximate solutions obtained by the AB, PAB and RFB methods when $c = 16.5\pi$.

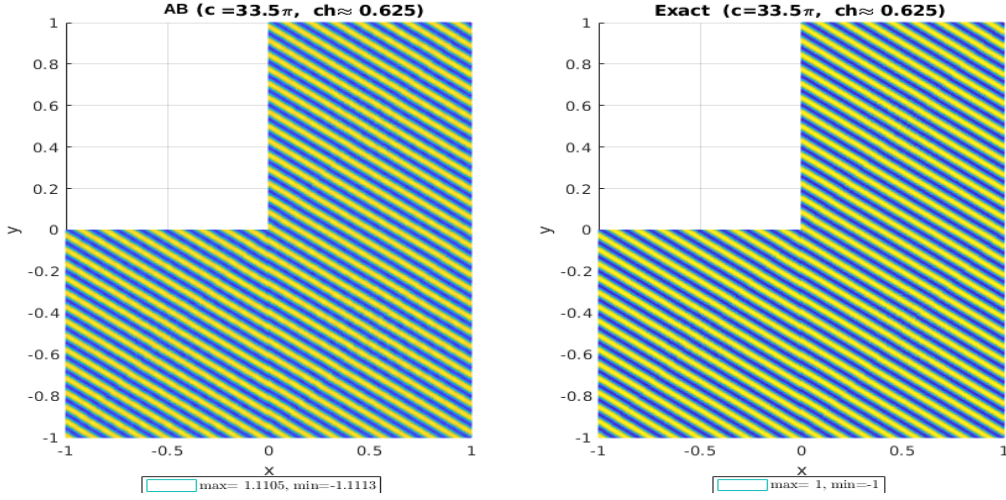


Figure 22: Contour plots of the approximate solutions obtained by the AB method and of the exact solutions on the same mesh when $c = 33.5\pi$.

6.5. Numerical test 5: A circular complex domain

In this test problem, we consider a complex domain which is obtained by the following Matlab code.

$$\left\{ \begin{array}{l} \text{model} = \text{createpde}(1); \\ \text{geometryFromEdges}(\text{model}, @\text{scatterg}); \\ \text{generateMesh}(\text{model}, 'GeometricOrder', 'linear', 'Hmax', 0.625/c, 'Hmin', 0.625/c); \end{array} \right. \quad (30)$$

While homogenous Neumann boundary condition is imposed on the outer boundary of the domain, i.e., $\frac{\partial u}{\partial x} = 0$, Dirichlet boundary condition is imposed on the inner boundary of the domain for which $u(x, y) = 0.1$. The right hand side of the problem is set to zero. The reference solution is obtained by standard Galerkin method on a fine mesh for which $ch \approx 0.09$. While Figure 23 shows the plots of the reference solution and approximate solutions of the AB, PAB and RFB method for $c = 3.5\pi$, Figure 24 shows for $c = 16.5\pi$. We see that the RFB method is worst in any case. Although the AB and PAB give similar results for smaller wave numbers, the AB method is better by far than the PAB for large wave numbers. This and the previous tests show the success of the AB method on complex domains with unstructured meshes.

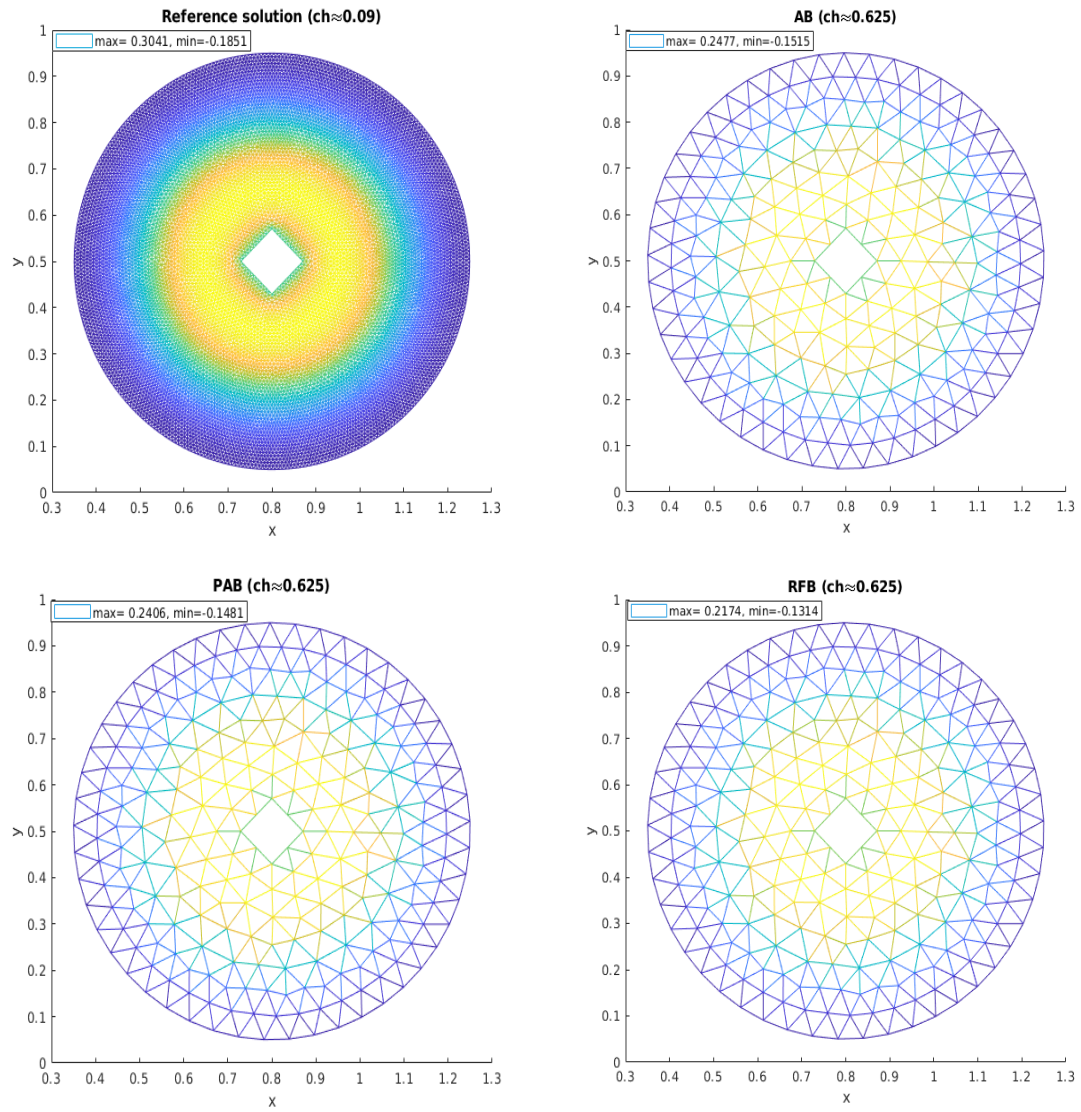


Figure 23: Plots of the reference solution and approximate solutions obtained by the AB, PAB and RFB methods when $c = 3.5\pi$.

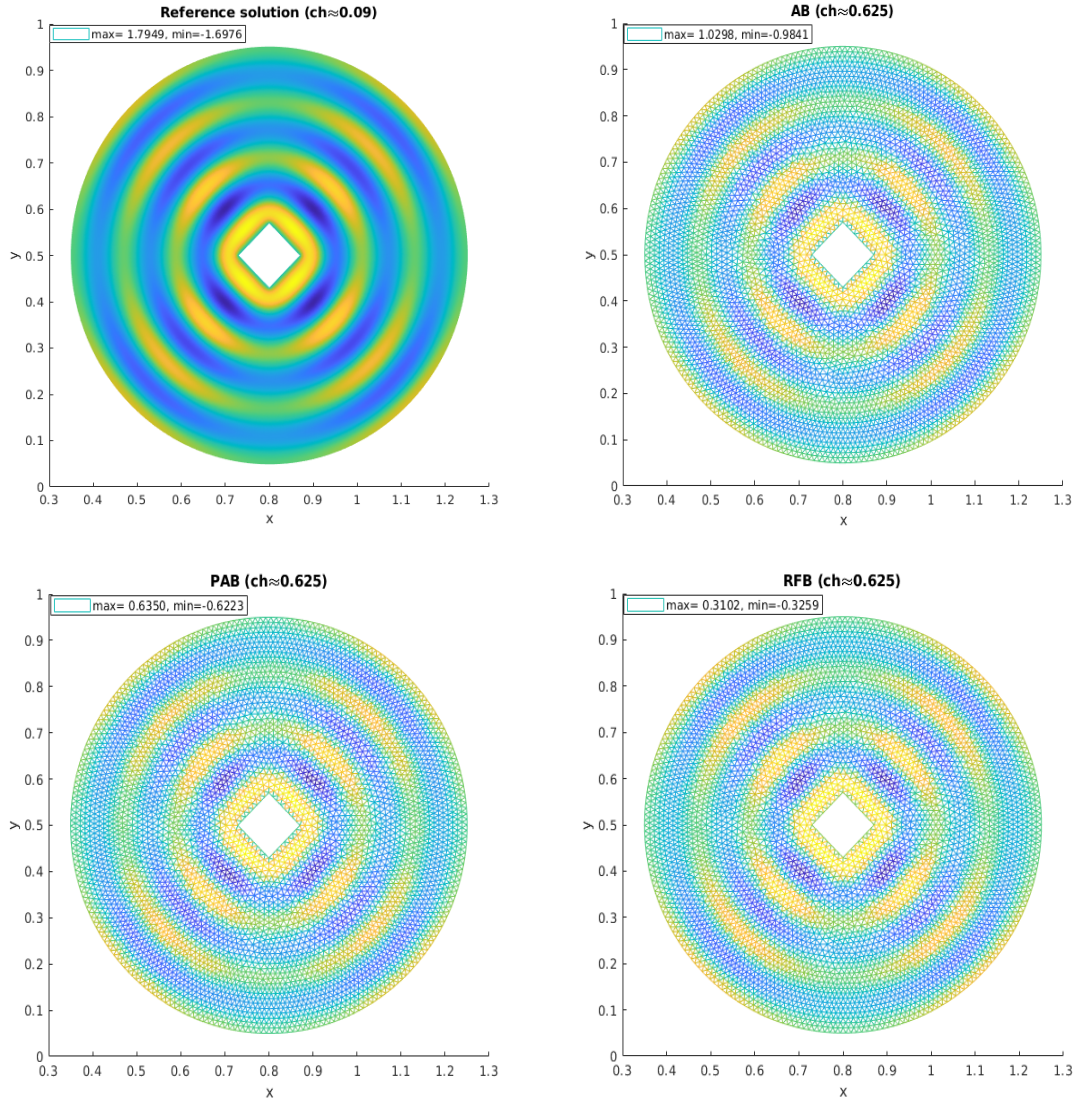


Figure 24: Plots of the reference solution and approximate solutions obtained by the AB, PAB and RFB methods when $c = 16.5\pi$.

7. Adaptive bubbles method with rectangular elements

Although the AB method is very effective with triangular elements, in some domains, rectangular elements may have some advantages such as in a rectangular region. For a rectangular element, there are five bubble equations to be solved.

$$\begin{cases} -\Delta\varphi_i - c^2\varphi_i = \mu c^2\psi_i & \text{in } K, \quad (i = 1, \dots, 4) \\ \varphi_i = 0 & \text{on } \partial K, \end{cases} \quad (31)$$

and

$$\begin{cases} -\Delta\varphi_f - c^2\varphi_f = f & \text{in } K, \\ \varphi_f = 0 & \text{on } \partial K, \end{cases} \quad (32)$$

where ψ_i ($i = 1, \dots, 4$) are the bilinear basis functions of a rectangular element. In this case, the constant that we multiply the right hand side of the bubble equation (31) is fixed for each bubble equations. We considered the Dirichlet problem (17) on unit square when $\theta = 0$ to find the optimal values (in infinity norm). We report the optimal values of μ for a squared shaped element for varying ch where $h = (h_1 + h_2 + h_3 + h_4)/4$ and h_i ($i = 1, \dots, 4$) are lengths of the edges of a rectangular element, in Table 2.

Remark 3. Note that the values in Table 2 are also optimal for $\theta = \pi$. It is possible to find the optimal values in any direction. However, triangular elements have some advantages.

- Rectangular elements use 9 points per degrees of freedom but triangular elements use 7 points per degrees of freedom.
- While rectangular elements require solving 5 different bubble equations, triangular elements require 4. This makes rectangular elements less efficient when nonuniform mesh is used.
- Triangular elements allow to work with larger ch .
- Triangular elements are more efficient on unstructured meshes.

Table 2: Optimal values of μ for rectangular elements for varying ch

ch	μ	N_s	ch	μ	N_s
≤ 0.94	2.5	8	1.72	2.8	10
1.02	2.6	8	1.80	2.85	10
1.09	2.6	8	1.88	2.88	10
1.17	2.6	8	1.96	2.88	10
1.25	2.65	8	2.04	2.98	10
1.33	2.65	8	2.12	3.05	10
1.41	2.7	8	2.19	3.09	10
1.49	2.7	8	2.27	3.15	10
1.49	2.7	10	2.35	3.2	10
1.57	2.72	10	2.43	3.25	10
1.64	2.75	10	2.51	3.29	10

We are able to find the optimal values of μ up to $ch \approx 2.5$. N_s in Table 2, is the number of nodes on each edges of a rectangular element. $N_s = 8$ for $ch \leq 1.49$ and $N_s = 10$ when $ch > 1.49$. While $N_s = 8$ amounts to solving

36×36 linear systems of equations, $N_s = 10$ amounts to solving 64×64 linear systems of equations on element level. When ch is between any of the successive two values in Table 2, we use linear interpolation to get μ . We provide one numerical test to show the performance of the AB.

Remark 4. When $ch \leq 0.94$, the optimal values in any direction are same. Note that in simulations, 10 nodes per wave are generally used which corresponds to $ch \approx 0.625$.

7.1. Test 1

We consider the following Helmholtz problem in 2D on an L-shaped domain (see Figure 25 (left)).

$$\begin{cases} -\Delta u - c^2 u = 0, & \text{in } \Omega, \\ u(x, y) = \sin(cx), & \text{on } \partial\Omega_D, \\ \frac{\partial u}{\partial \mathbf{n}} = 0, & \text{on } \partial\Omega_N. \end{cases} \quad (33)$$

147 uniform square shaped elements are used for the decomposition of the domain (see Figure 25 (right)). Exact solution of this problem is $u(x, y) = \sin(cx)$.

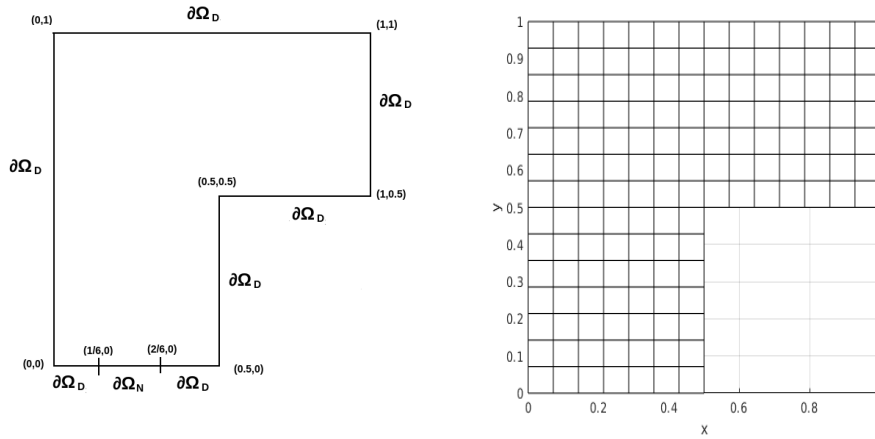


Figure 25: Domain of the problem (33) (left) and its decomposition with square elements (right).

We assess the performance of the AB method by comparing with the exact solution. Figure 26 represents the contour plots of the approximate and of the exact solutions for $ch = 2.46$. We also report the maximum and minimum values of the approximate and exact solutions. Results show that the AB method is very effective up to $ch = 2.5$ on uniform mesh.

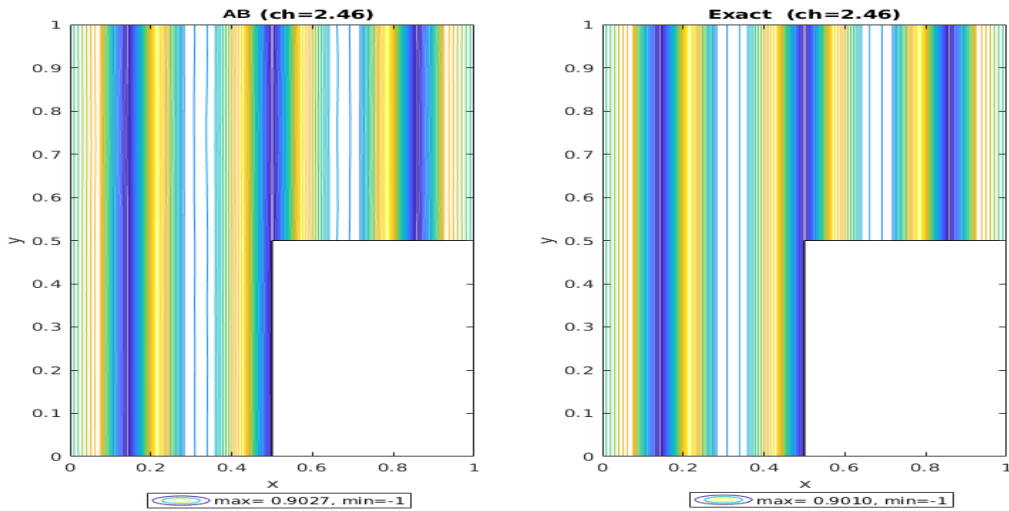


Figure 26: Contour plots of the approximate solutions obtained by the AB method and of the exact solutions when $ch = 2.46$.

8. Conclusion

In this article, we proposed an adaptive bubble approach for the Helmholtz equation in 2D. The RFB method requires obtaining the bubble functions which is generally as difficult as solving the original problem. We showed that this is not the case for the Helmholtz problem. The standard Galerkin finite element method can be used as a solver to obtain approximations to the bubble functions. In other words, the bubbles method does not depend on another stabilized method when applied to the Helmholtz problem. We showed that the contribution of the RFB method in stabilization of the standard Galerkin method is very poor in 2D. We modified the RFB method by multiplying the right hand-side of the bubble problems with a constant. We reported the optimal values of this constant for equilateral triangular elements. Various numerical experiments proved the robustness of the AB method in terms of the parameters provided. The AB method is able to solve the Helmholtz problem in 2D up to $ch = 3.5$, efficiently. The numerical tests showed that the AB method is by far better than the pseudo-adaptive bubbles method and the fourth order method. We provided analysis to prove that the AB method mitigates the pollution error substantially.

References

- [1] G. B. Alvarez, A. F. D. Loula, E. G. Dutra do Carmo, and F. A. Rochinha. A discontinuous finite element formulation for Helmholtz equation. *Comput. Methods Appl. Mech. Engrg.*, 195(33-36):4018–4035, 2006.
- [2] I. M. Babuška and S. A. Sauter. Is the pollution effect of the FEM avoidable for the Helmholtz equation considering high wave numbers? *SIAM J. Numer. Anal.*, 34(6):2392–2423, 1997.
- [3] F. Brezzi and A. Russo. Choosing bubbles for advection-diffusion problems. *Math. Models Methods Appl. Sci.*, 4(4):571–587, 1994.

- [4] S. Congreve, P. Houston, and I. Perugia. Adaptive refinement for hp -version Trefftz discontinuous Galerkin methods for the homogeneous Helmholtz problem. *Adv. Comput. Math.*, 45(1):361–393, 2019.
- [5] H. C. Elman, O. G. Ernst, and D. P. O’Leary. A multigrid method enhanced by Krylov subspace iteration for discrete Helmholtz equations. *SIAM J. Sci. Comput.*, 23(4):1291–1315, 2001.
- [6] Y. A. Erlangga, C. W. Oosterlee, and C. Vuik. A novel multigrid based preconditioner for heterogeneous Helmholtz problems. *SIAM J. Sci. Comput.*, 27(4):1471–1492, 2006.
- [7] O. G. Ernst and M. J. Gander. Why it is difficult to solve Helmholtz problems with classical iterative methods. In *Numerical analysis of multiscale problems*, volume 83 of *Lect. Notes Comput. Sci. Eng.*, pages 325–363. Springer, Heidelberg, 2012.
- [8] X. Feng, Z. Li, and Z. Qiao. High order compact finite difference schemes for the Helmholtz equation with discontinuous coefficients. *J. Comput. Math.*, 29(3):324–340, 2011.
- [9] X. Feng and H. Wu. Discontinuous Galerkin methods for the Helmholtz equation with large wave number. *SIAM J. Numer. Anal.*, 47(4):2872–2896, 2009.
- [10] L. P. Franca, C. Farhat, A. P. Macedo, and M. Lesoinne. Residual-free bubbles for the Helmholtz equation. *Internat. J. Numer. Methods Engrg.*, 40(21):4003–4009, 1997.
- [11] L. P. Franca and A. P. Macedo. A two-level finite element method and its application to the Helmholtz equation. *Internat. J. Numer. Methods Engrg.*, 43(1):23–32, 1998.
- [12] L. P. Franca, A. Nesliturk, and M. Stynes. On the stability of residual-free bubbles for convection-diffusion problems and their approximation by a two-level finite element method. *Comput. Methods Appl. Mech. Engrg.*, 166(1-2):35–49, 1998.
- [13] L. P. Franca and A. Russo. Deriving upwinding, mass lumping and selective reduced integration by residual-free bubbles. *Appl. Math. Lett.*, 9(5):83–88, 1996.
- [14] L. P. Franca and A. Russo. Unlocking with residual-free bubbles. *Comput. Methods Appl. Mech. Engrg.*, 142(3-4):361–364, 1997.
- [15] M. J. Gander, F. Magoulès, and F. Nataf. Optimized Schwarz methods without overlap for the Helmholtz equation. *SIAM J. Sci. Comput.*, 24(1):38–60, 2002.
- [16] F. Ihlenburg and I. M. Babuška. Finite element solution of the Helmholtz equation with high wave number. I. The h -version of the FEM. *Comput. Math. Appl.*, 30(9):9–37, 1995.
- [17] S. Kirkup. The boundary element method in acoustics: A survey.
- [18] Matlab. *version 9.8.0.1380330 (R2020a)*. The MathWorks Inc., Natick, Massachusetts, 2021.
- [19] A. I. Nesliturk. *Approximating the incompressible Navier-Stokes equations using a two-level finite element method*. ProQuest LLC, Ann Arbor, MI, 1999. Thesis (Ph.D.)—University of Colorado at Denver.
- [20] I. Perugia, P. Pietra, and A. Russo. A plane wave virtual element method for the Helmholtz problem. *ESAIM Math. Model. Numer. Anal.*, 50(3):783–808, 2016.
- [21] A. Sendur, A. Nesliturk, and A. Kaya. Applications of the pseudo residual-free bubbles to the stabilization of the convection-diffusion-reaction problems in 2D. *Comput. Methods Appl. Mech. Engrg.*, 277:154–179, 2014.
- [22] A. Sendur and A. I. Nesliturk. Applications of the pseudo residual-free bubbles to the stabilization of convection-diffusion-reaction problems. *Calcolo*, 49(1):1–19, 2012.
- [23] I. Singer and E. Turkel. High-order finite difference methods for the Helmholtz equation. *Comput. Methods Appl. Mech. Engrg.*, 163(1-4):343–358, 1998.
- [24] C. C. Stolk. A rapidly converging domain decomposition method for the Helmholtz equation. *J. Comput. Phys.*, 241:240–252, 2013.
- [25] T. Strouboulis, I. M. Babuška, and R. Hidajat. The generalized finite element method for Helmholtz equation: theory, computation, and open

problems. *Comput. Methods Appl. Mech. Engrg.*, 195(37-40):4711–4731, 2006.